Mutual Impedance Matrix Extraction from Embedded Element Patterns of the Murchison Widefield Array

Maria Kovaleva*(1), Georgios Kyriakou(2), and David B. Davidson(1)
(1) International Centre for Radio Astronomy Research (ICRAR-Curtin), 1 Turner Avenue, Bentley, WA 6102, Australia
(2) INAF-Arcetri Astrophysical Observatory, Largo Enrico Fermi 5, 50125, Florence, Italy, georgios.kyriakou@inaf.it

Abstract

Low frequency aperture arrays for radio astronomy, one of which is the Murchison Widefield Array, are at the forefront of modern radio astronomy aiming to expand our knowledge on the universe by low-frequency science. Due to the high density of aperture arrays at the low end of the operating spectrum, strong mutual coupling is a concern. While the embedded element patterns of deployed prototypes can and have been measured using unmanned aerial vehicles, traditional direct measurements of the mutual impedance matrix are not feasible. This paper addresses the issue using a recently introduced method of mutual impedance matrix extraction from simulated array embedded element patterns. Through an iterative optimisation process, mutual impedance matrices at five frequency points within the 70-300 MHz range were extracted with a very low relative error, confirming the robustness of the method.

1 Introduction

Low-frequency radio astronomy (below 500 MHz) uses aperture arrays as its RF front-ends. Major science goals that motivate the development of radio astronomy at low frequencies concern the search for the redshifted hydrogen emission from the early universe, extragalactic surveys, high-energy transient sources and ultra-high energy cosmic rays [1]. Large multipurpose radio telescopes that have been delivering observational data to radio astronomers around the world for more than a decade include the Low-Frequency Array (LOFAR) in Europe, the Long Wavelength Array (LWA) in the United States and the Murchison Widefield Array (MWA) in Australia. The latter is located on the Murchison Radio Astronomy Observatory (MRO) in the state of Western Australia. It is a designated precursor of the low-frequency component of the Square Kilometre Array (SKA-Low).

Measuring the performance of deployed antennas comprising radio telescopes is a time-demanding and expensive procedure due to the large number of antenna elements. Instead, in radio astronomy, the received power as a function of time plot (raw data) usually serves as a primary indicator of array performance. Recently, a technique for obtaining scattering parameters or a mutual impedance matrix from radiation patterns was proposed [2]. Combined with the unmanned aerial vehicle (UAV) measurements of embedded element patterns (EEPs) previously conducted on a subarray of MWA dipoles [3] and SKA-Low station prototypes [4], this technique offers a solution for an indirect measurement of mutual coupling and self-impedance in aperture arrays.

In this paper, we present an application of the method for the mutual impedance matrix (MIM) extraction from simulated EEPs applied on an MWA tile. Section 2 provides a description of the antenna array and the characteristics of its MIM. The method of MIM extraction (MIME) is given in Section 3, and the results are shown in Section 4.

2 MWA Tile: 16-Element Planar Array

MWA has been in operation since 2013, and its system was extensively characterised [5, 6, 7]. Here, we provide only the design parameters relevant to this work. MWA antennas are dual-polarised wideband bow-tie dipoles with differential-input low-noise amplifiers (LNA) connected to each antenna input and fitted inside UV-resistant hubs that hold the antenna arms. The dipole is optimised to operate in the 70-300 MHz frequency range, with its length (L) and width (W) being 0.74 m and 0.4 m, respectively, as shown in Figure 1.

The distance (H) from the antenna arms to the metallic ground screen is below 0.1λ over the entire frequency range. Arranged in a 4-by-4 planar configuration on a 5x5 m ground screen, MWA dipoles create a 16-element MWA tile. Dipole separation (d) is 1.1 m, which corresponds to half a wavelength at 136 MHz. Since MWA is a wideband array, its electrical lengths vary significantly over the operating frequency range. Its dimensions in terms of wavelengths are shown in Figure 2.

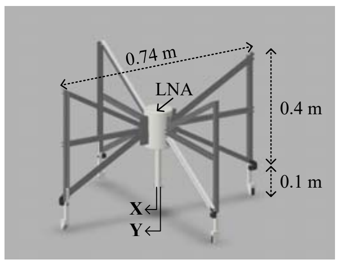

Figure 1. MWA dipole CAD model.

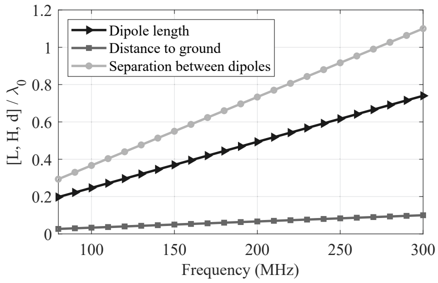

Figure 2. MWA dimensions in electrical lengths: dipole length $L = 0.74$ m, distance to the ground screen $H = 0.1$ m and separation $d = 1.1$ m.

Aperture arrays are subject to strong mutual coupling, especially when the dipole separation is electrically small (dense arrays). To capture the effect of antenna interactions within an array, EEPs are computed [10]. If mutual coupling is strong, EEPs differ significantly from the radiation pattern of an isolated element. In the MWA, mutual coupling appears stronger at frequencies below 136 MHz. Figure 3 shows the range of resistance and reactance for both self-impedance ($\mathbf{Z}_A^{ii}$) and mutual coupling ($\mathbf{Z}_A^{ij}$) as a function of frequency. The minimum and maximum values of $\mathbf{Z}_A^{ii}$ are very similar, which means that the input impedance remains fairly constant for all array elements at the same frequency. Figure 4 shows the real and imaginary components of $\mathbf{Z}_A$ at 154.88 MHz, visualising that for all antennas, self impedance is about $\mathbf{Z}_A^{11} = 68 + 158j\ \Omega$, and mutual coupling $\mathbf{Z}_A^{ij} = (-6.5...25) + (-20...7)j\ \Omega$.
Due to reciprocity, the MIM is a symmetric matrix, and therefore, only the upper or lower triangle can be considered as an unknown parameter in the optimisation procedure described in Section 3. Also, we observed that due to the symmetry of the MWA tile, the EEPs of the elements at the same distance from the symmetry plane and aligned on the x- or y-axis are the same in the principal planes.

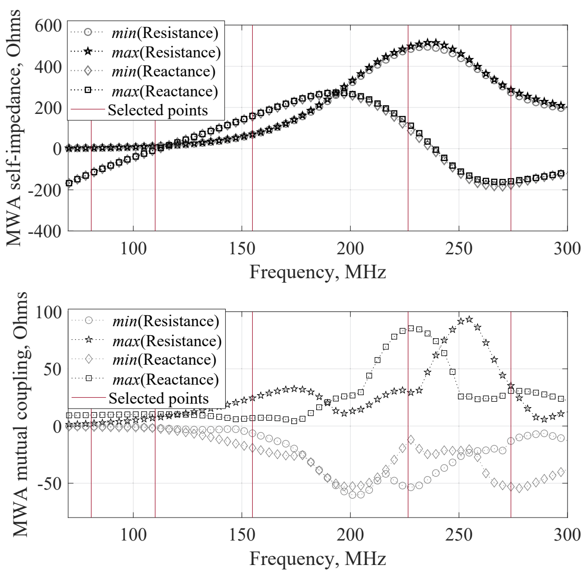

Figure 3. FEKO-simulated MWA tile impedance.

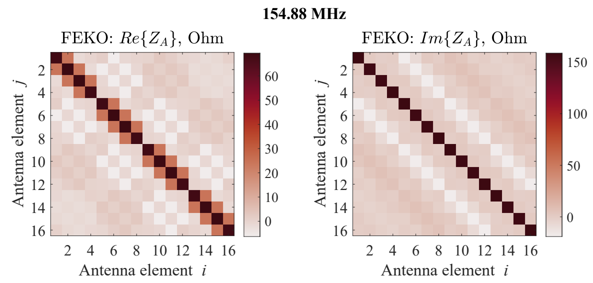

Figure 4. MIM for an MWA tile in X polarisation at 154.88 MHz.

3 MIM Extraction (MIME) Method

Mutual coupling between antenna elements changes the EEPs, and therefore, it is important to know the exact EEPs of all elements in an array. In modern array applications, phased arrays represent a very common technology, and for this reason, mutual coupling is a subject of increased research interest [9, 10]. In low-frequency radio astronomy, EEPs are crucial for accurate calibration and beamforming. It is well-known that EEPs obtained for different termination conditions, such as $\mathbf{E}^{\mathbf{Z}_{L2}}$ and $\mathbf{E}^{\mathbf{Z}_{L1}}$, are related by the array impedance matrix $\mathbf{Z}_A$ and the diagonal load matrices $\mathbf{Z}_{L1} = Z_{L1}\mathbf{I}$ and $\mathbf{Z}_{L2} = Z_{L2}\mathbf{I}$ as:

$$\mathbf{E}^{\mathbf{Z}_{L2}} = (\mathbf{Z}_A + \mathbf{Z}_{L2})^{-\mathrm{T}}(\mathbf{Z}_A + \mathbf{Z}_{L1})^{\mathrm{T}}\mathbf{E}^{\mathbf{Z}_{L1}} \quad (1)$$

An LNA-loaded MWA tile was simulated in FEKO to generate EEPs for X and Y polarisations. Frequency-dependent LNA impedance is represented by an equivalent circuit from the previous measurements. As shown in [8], the pattern transformation given in Eq. (1) was previously used to accurately calculate EEPs for faulty LNAs.
The MIME procedure was performed for five randomly selected frequency points: (1) 80.64 MHz, (2) 110.08 MHz, (3) 154.88 MHz, (4) 226.56 MHz and (5) 273.92 MHz, which are marked by vertical lines in Figure 3. This method includes the steps described below.

1. Obtain EEPs ($\mathbf{E}^{\mathbf{Z}_L}$) for $\mathbf{Z}_L$-terminated array via electromagnetic simulations or measurements.

2. Convert $\mathbf{E}^{\mathbf{Z}_L}$ to open-circuit (OC) and short-circuit (SC) EEPs with Z_0-impedance Thévenin sources ($\mathbf{E}^{\mathrm{oc,th}}$ and $\mathbf{E}^{\mathrm{sc,th}}$) according to:

$$\mathbf{E}^{\mathrm{oc,th}} = Y_0(\mathbf{I} + Y_0\mathbf{Z}_{A,d})^{-1}(\mathbf{Z}_A + \mathbf{Z}_L)\mathbf{E}^{\mathbf{Z}_L} \quad (2)$$

$$\mathbf{E}^{\mathrm{sc,th}} = (\mathbf{I} + Z_0\mathbf{Y}_{A,d})^{-1}\mathbf{Z}_A^{-1}(\mathbf{Z}_A + \mathbf{Z}_L)\mathbf{E}^{\mathbf{Z}_L}. \quad (3)$$

3. Optimise the goal function to generate $\hat{\mathbf{Z}}_A$ using the short-circuit to open-circuit Thévenin-source transformation equation:

$$\mathbf{E}^{\mathrm{oc,th}} = Y_0(\mathbf{I} + Y_0\mathbf{Z}_{A,d})^{-1}\mathbf{Z}_A(\mathbf{I} + Z_0\mathbf{Y}_{A,d})\mathbf{E}^{\mathrm{sc,th}} \quad (4)$$

   More details about loading condition transformations with an arbitrary Thévenin source can be found in [2].

The MIME is an iterative-solution technique utilising an optimisation algorithm. Therefore, any solution it produces is prone to a numerical error. We are evaluating the performance of MIME by the relative error:

$$\Delta \mathbf{Z}_A = \frac{||\mathbf{Z}_A - \hat{\mathbf{Z}}_A||_F}{||\mathbf{Z}_A||_F}, \tag{5}$$

where "F" refers to the Frobenius norm, and $\mathbf{Z}_A$ is a FEKO-simulated impedance matrix.

Electric field samples in the above definitions were also generated in FEKO and stored in an array with columns corresponding to different zenith angles, and rows corresponding to antenna element numbers. As of now, it has not yet been determined what the optimal resolution of the EEPs is or what the optimal ranges of zenith and azimuth angles should be. Due to the limitation of the maximum zenith angle in UAV measurements, it would be useful to further investigate this question.

4 Results

The MIM is a matrix of complex numbers. To apply the described procedure, we separated real and imaginary components and treated them as separate variables. The real-number numerical optimisation is much more developed, and therefore, it is a common strategy to transform complex values into real numbers. To reduce the problem dimensionality, we optimised only the lower triangle and the diagonal of the impedance matrix. Thus, the vector of unknown parameters has 272 variables. The goal function was minimised using `fmincon` algorithm in MATLAB.

We found that for MWA, both co-polarised and cross-polarised field components are necessary to achieve accurate $\hat{\mathbf{Z}}_A$. Without the cross-polarised components, relative error $\Delta\mathbf{Z}_A$ was higher than 20%, even though the algorithm converged. We concatenated co-polarised and cross-polarised E-fields in two principal planes in a (16-by-364) array of $[E^{\theta}_{(\varphi=0^\circ)}, E^{\theta}_{(\varphi=90^\circ)}, E^{\varphi}_{(\varphi=0^\circ)}, E^{\varphi}_{(\varphi=90^\circ)}]$. Figure 5 shows concatenated OC-Thévenin EEPs generated by Eq. (4) using $\mathbf{Z}_A$ (solid line) and $\hat{\mathbf{Z}}_A$ (dashed line) at 273.92 MHz. The agreement of the EEPs confirms the accuracy of the extracted $\hat{\mathbf{Z}}_A$. As discussed earlier, the MWA tile is a symmetrical array, and therefore, only eight EEPs can be seen on the figure due to the overlap of identical EEPs. For each of the selected frequencies, an optimisation routine was performed 10 times with a random restart to confirm the robustness of the method. On a Windows laptop with 13th Gen Intel i7-1362 processor with 64 GB of RAM, the average time for one complete MIME run is 6 mins. The algorithm produces a low relative error when the goal function reaches the level of 10^{-5}.

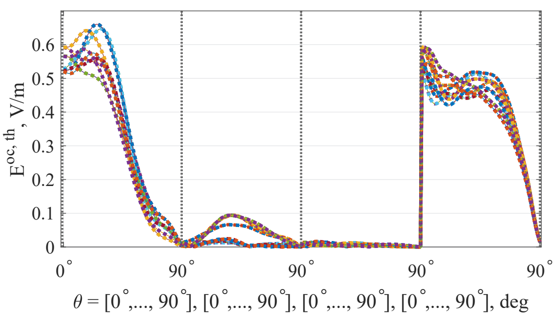

Figure 5. Concatenated co-polarised and cross-polarised E-fields in two principal planes for 273.92 MHz. Solid line shows $\mathbf{E}^{\text{oc,th}}$ generated by Eq. (2), dashed line shows $\mathbf{E}^{\text{oc,th}}$ calculated using $\hat{\mathbf{Z}}_A$ and Eq. (4).

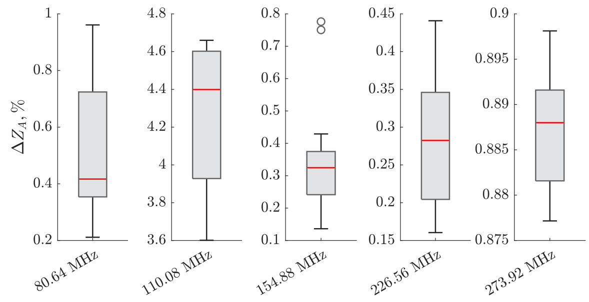

Figure 6. Box and whisker plot for the relative errors of MIME (results of 10 runs) for the selected frequency points. Red line indicates the median values, grey box indicates lower and upper quartile.

Figure 6 represents the main result of this work. Relative error is less than 5% for all frequency points and less than 1% for all but 110.08 MHz. We noticed that the optimiser did not perform well for 110.08 MHz problem. It can be attributed to the fact that the resistance and reactance of $\mathbf{Z}^{ii}_A$ and $\mathbf{Z}^{ij}_A$ in this MIM is close to zero, which made it harder for `fmincon` to converge. This can be rectified by using another optimisation method or limiting the maximum step size, but this problem should be noted for further applications. Nevertheless, the obtained $\Delta\mathbf{Z}_A$ confirms that MIME can be an accurate alternative method for "measuring" $\mathbf{Z}_A$ when antenna ports cannot be directly accessed, such as in integrated antennas, or when the number of antenna ports is significantly larger than the number of ports in the vector network analyser, such as in phased arrays for radio astronomy and MIMO applications.

5 Conclusion

We demonstrated that the MIME technique produces very reliable solutions for the array impedance matrices from the simulated EEPs through an iterative optimisation process. We used a 16-element array that is called tile in an MWA radio telescope and extracted mutual impedance matrices at five randomly selected frequency points. The procedure only takes about 6 mins and typically, returns a solution with less than 1% relative error if simulated noiseless radiation patterns are used. The next step in this project would be to use UAV-measured EEPs to verify that the MIME can also be accurate for "noisy" EEPs.

6 Acknowledgements

We acknowledge the Wajarri Yamatji people as the traditional owners of the Murchison Radio Astronomy Observatory site.

References

[1] M. de Vos, "LOFAR: the first of a new generation of radio telescopes," *Proceedingsof the IEEE International Conference On Acoustics, Speech, and Signal Processing*, **5**, pp. 865-868, Vol.5, 2005

[2] Buck, D., Warnick, K., Maaskant, R., Davidson, D. & Kelley, D., "Measuring Array Mutual Impedances Using Embedded Element Patterns," *IEEE Transactions On Antennas And Propagation*. **71**, pp. 606-611, 2023

[3] Paonessa, F., Ciorba, L., Virone, G., Bolli, P., Monari, J., Perini, F., Wayth, R., Sutinjo, A. & Davidson, D., "Characterization of the Murchison Widefield Array Dipole with a UAV-mounted Test Source," *13th European Conference On Antennas And Propagation (EuCAP)*. pp. 1-4, 2019

[4] Paonessa, F., Ciorba, L., Kyriakou, G., Bolli, P. & Virone, G. UAV-Based Measurement of Sharp Spectral Resonances in Mutually Coupled SKA-Low Elements. *IEEE Antennas And Wireless Propagation Letters*. **22**, 2735-2739 (2023)

[5] S. J. Tingay et al., "The Murchison Widefield Array: The Square Kilometre Array Precursor at Low Radio Frequencies," *Publications of the Astronomical Society of Australia*, **30**, e007, 2013

[6] R. B. Wayth et al., "The Phase II Murchison Widefield Array: Design overview," *Publications of the Astronomical Society of Australia*, **35**, e033, 2018

[7] A. T. Sutinjo, D. C. X. Ung and B. Juswardy, "Cold-Source Noise Measurement of a Differential Input Single-Ended Output Low-Noise Amplifier Connected to a Low-Frequency Radio Astronomy Antenna," *IEEE Transactions on Antennas and Propagation*, **66**, no. 10, pp. 5511-5520, Oct. 2018

[8] M. Kovaleva et al., "Analysis of the Loading Effect of Faulty LNAs on Embedded Element Patterns in the Murchison Widefield Array," *14th European Conference on Antennas and Propagation*, Copenhagen, Denmark, pp. 1-4, 2020

[9] C. Craeye, H. Van, "Methods for Analyzing Mutual Coupling in Large Arrays," *Mutual Coupling Between Antennas*. pp. 369-387, 2021

[10] K. F. Warnick, R. Maaskant, M. V. Ivashina, D. B. Davidson, and B. D. Jeffs, "Phased Arrays for Radio Astronomy, Remote Sensing, and Satellite Communications," Cambridge University Press, 2018.